A GIS-based flood risk mapping of Assam, India, using the MCDA-AHP approach at the regional and administrative level

Laxmi Gupta
Shiv Nadar University
Jagabandhu Dixit (jagabandhu.dixit@snu.edu.in)
Shiv Nadar University

Research Article

Keywords: Flood hazard, vulnerability, risk, GIS, analytical hierarchy process (AHP), multicriteria decision analysis (MCDA), Assam

Posted Date: October 25th, 2021

DOI: https://doi.org/10.21203/rs.3.rs-1015728/v1

Version of Record: A version of this preprint was published at Geocarto International on March 30th, 2022. See the published version at https://doi.org/10.1080/10106049.2022.2060329.

A GIS-based flood risk mapping of Assam, India, using the MCDA-AHP approach at the regional and administrative level

Laxmi Gupta, Jagabandhu Dixit*

Disaster Management Laboratory, Shiv Nadar University, Delhi NCR, Greater Noida, Uttar Pradesh 201314, India

E-mail address of authors: lg100@snu.edu.in; jagabandhu.dixit@snu.edu.in

***Corresponding Author:** Jagabandhu Dixit, Email: jagabandhu.dixit@snu.edu.in

Abstract

Floods are hydrological disasters that can alter the physical, socioeconomic, and environmental settings of a region. The objective of the present study is to develop an efficient and reliable methodology to prepare a flood risk map for Assam, the North-eastern region (NER) of India, by the integration of hazard and vulnerability components. Three indices, namely flood hazard index (FHI), flood vulnerability index (FVI), and flood risk index (FRI), are developed using multi-criteria decision analysis (MCDA) – Analytical hierarchy process (AHP) approach in GIS environment for the regional and administrative level of Assam. The selected hazard and vulnerability indicators define the topographical, geological, meteorological, drainage characteristics, land use land cover, and demographical features of Assam. The results show that more than 70% of the total area lies in the moderate to very high FHI class, 57.37% have moderate to high FVI, and more than 50% have moderate to very high FRI class.

Keywords: Flood hazard, vulnerability, risk, GIS, analytical hierarchy process (AHP), multicriteria decision analysis (MCDA), Assam.

1. Introduction

Natural disasters are caused by geological, hydrological, and meteorological events resulting in immeasurable loss of lives and property and natural landscape damage. Flood is the most

frequent and expensive hydro-meteorological hazard due to its high intensity of damage (Tabarestani and Afzalimehr 2021). Over the past few decades, the frequency of flood and its extent of destruction have increased significantly due to uneven distribution of rainfall, rapid snow melting, overflow of rivers, deforestation, uncontrolled urbanization, and unplanned human settlement along the coastal areas and riverbanks (Armenakis et al. 2017). From 2000 to 2019, floods contributed 44% of the total disaster worldwide, and Asia alone experiences 41% of the total flood events of the world, affecting approximately 1.5 billion people (CRED 2020). The intensity of flood varies temporally and spatially, and its occurrence and negative consequences cannot be prevented altogether (Dewan et al. 2006). As developing countries are more vulnerable to floods, there is an urgent need to assess and manage future flood events to minimize the adverse impact. Flood management at the regional or local scale begins with identifying vulnerable areas, detailed understanding of interaction and relationships among the social, economic, and environmental factors to provide the rescue and mitigation response in case of emergency. A comprehensive flood risk map is a critical tool for executing an effective flood management system (Chakrabortty et al. 2021).

Many studies have been conducted on flood assessment at the regional, national, and global levels using different approaches and methodologies (Chen et al. 2015; Kumar 2016; Majumder et al. 2019; Sharma et al. 2019; Toosi et al. 2019). The studies have inherent challenges and limitations in identifying and quantifying hazard and vulnerability indicators, dealing with uncertainties, assigning a proper weightage of indicators, and validating the result (Sharma et al. 2018; Arora et al. 2021). The indicators involved in the risk assessment are complex and contain temporal and spatial uncertainties (Choubin et al. 2019). The main challenge is acquiring and collecting data of the selected indicators (Mishra and Sinha 2020). Over the past few decades, remote sensing has played a crucial role in monitoring floods, and it has also solved the challenges related to the availability of data (Sharma et al. 2018; Wang

50 and Xie 2018; Rong et al. 2020). In recent times, GIS has been widely used in vulnerability
51 and risk assessment studies as a decision support system for its database and analytical ability
52 (Lyu et al. 2018; Choubin et al. 2019; Danso et al. 2020).

53 Armenakis et al. (2017) developed a flood risk map for the Don River watershed, Toronto,
54 using high spatial resolution data and incorporated demographic indicators to enhance
55 mitigation and preparedness planning. Dandapat and Panda (2017) delineated the flood risk
56 zone of Paschim Medinipur in West Bengal, India, and developed a composite vulnerability
57 index, comprising of i) Physical Vulnerability Index, ii) Social Vulnerability Index, and iii)
58 Coping Capacity Index within the GIS framework and estimated that 24.25% of the total
59 population of the study area is located in high to very high flood risk zones. Sharma et al.
60 (2018), using multicriteria analysis (MCA) and geospatial technique, carried out a flood risk
61 assessment for Kopili River Basin (KRB) in Assam, India, and estimated that a significant
62 portion of the crop and village land falls under high and moderate flood risk zones respectively.
63 Arora et al. (2019) applied Shannon's entropy (SE) and frequency ratio (FR) models to build a
64 flood susceptibility model for Middle Ganga Plain using the 2008 Landsat 5TM image.
65 Khosravi et al. (2020) developed a national scale flood susceptibility map for Iran using a deep
66 learning convolutional neural networks (CNN) algorithm and illustrate the importance of
67 watershed management and prevention of uncontrolled urban expansion to control flood.
68 Zhang et al. (2020) developed a GIS-based model for flood risk assessment at a large basin
69 scale, such as the Yangtze River Basin, China, taking economic, social, and ecological
70 indicators of flood risk.

71 Several researchers have done GIS-based flood vulnerability studies using multiple approaches
72 (Hazarika et al. 2018; Brito et al. 2019; Dekongmen et al. 2021). Rashetnia and Jahanbani
73 (2021) developed a GIS- fuzzy rule-based flood vulnerability index for Moreland city,
74 Melbourne, considering social, economic, and hydrological factors. Sadeghi-Pouya et al.

(2017) carried out a flood vulnerability assessment of the western coastal cities of Mazandaran Province, Iran, by classifying effective criteria into three indices, i.e., socio-economic, population-environmental, and technical. Sarkar and Mondal (2020) performed a GIS-based flood vulnerability classification of the Kulik river basin using the frequency ratio (FR) model.

Detailed flood risk assessment has been carried out by incorporating hazard and vulnerability assessment and hydrological models (Vojtek and Vojteková 2019; Sharma et al. 2018; Pathak et al. 2020). The essential factor in flood risk assessment is the proper weightage assignment to the selected indicators. Many studies have applied Multi-Criteria Decision Analysis (MCDA) to identify, integrate, or rate the flood risk assessment factors (Chen et al. 2015; Arabameri et al. 2019; Toosi et al. 2019; Mishra and Sinha 2020). Chakraborty and Mukhopadhyay (2019) integrated AHP and GIS for the development of flood risk map for Coochbehar district, West Bengal, India, by the quantification of flood risk index (FRI) using flood hazard index (FHI) and flood vulnerability index (FVI). Hazarika et al. (2018) explained that the application of multicriteria analysis in the GIS environment provides flexibility in selecting significant indicators for the flood risk assessment for Dhemaji district in the Upper Brahmaputra River valley Assam, India.

India is considered the second most flood-affected country globally, following China, and it experiences about 17 flood events per year on average, affecting approximately 345 million people (CRED 2020). The vast river network system and the world's most prominent monsoon system make about 5.74 million hectares of the total land area inundated by floods (Subrahmanyam 1988; Dhar and Nandargi 2004). The issue of flood risk is quite prominent in the Assam region of India due to the highly braided Brahmaputra River. It is mainly influenced by the southwest tropical monsoon, making the river experiencing high water levels and strong flows in the pre-monsoon season. Apart from topographic and meteorological factors, other factors like population settlement along the flood plains, erosion, and siltation of the banks

100 accelerate the flood problem in the Brahmaputra basin. Every year the region suffers enormous
101 losses and damage in terms of property and lives, so there is an urgent need to conduct a
102 comprehensive food risk assessment and identify vulnerable areas and triggering factors.
103 The flood-related study for the Assam region is limited only to one aspect like hazard,
104 vulnerability, or risk focussing only on a small area, river basin, or district level with a limited
105 number of indicators (Borah et al. 2018; Hazarika et al. 2018; Sharma et al. 2018; Majumder
106 et al. 2019; Pathan and Sil 2020; Sarmah et al. 2020; Pareta 2021). Considering hazard and
107 vulnerability aspects, comprehensive flood risk assessment studies for the entire Assam region
108 are limited. In the present study, a GIS-based comprehensive flood risk assessment of the
109 Assam region at a regional scale and administrative level is conducted by integrating spatial,
110 hydrological, and socio-economic indicators. The weightage of each indicator is determined
111 by the application of the MCDA technique. The final hazard and risk maps are validated by
112 confusion matrix or error matrix, indirect methods of relative mean error (RME), and root of
113 mean-square error (RMSE) based on historical flood events. The study framework provides an
114 opportunity to understand the challenges associated with flood risk management and to
115 implement effective and sustainable flood mitigation measures and policies for urban and rural
116 areas located at flood risk zones.
117 The main objectives of the present study are as follows i) to develop a GIS-based flood hazard,
118 vulnerability, and risk index by the selection of suitable hazard and vulnerability indicators,
119 weighted according to their significance, ii) to produce high-resolution flood risk, hazard, and
120 vulnerability maps by integrating MCDA and GIS to identify flood-prone areas, iii) to analyze
121 the flood risk scenario at the administrative level.

122 **2. Study area**

123 Assam lies in the north-eastern region (NER) of India, covering an area of approximately
124 78,438 km^2, extending from 24° 8′ N to 28° 2′ N latitude and 89° 42′ E to 96° E longitude. The

125 elevation of the Assam region ranges from 5-1964 m. The neighbouring states of Assam are
126 West Bengal, Arunachal Pradesh, Nagaland, Manipur, Mizoram, Tripura, and Meghalaya.
127 Assam shares its boundary with neighboring countries, Bhutan in the north and Bangladesh in
128 the south (Figure 1). The Guwahati city of Assam, the largest metropolis in NER, is known as
129 the "Gateway to Northeast India" and connects the entire NER with the rest of India. The
130 geographical feature of Assam contains three major physiographic divisions of India i) the
131 northern Himalayas as Eastern hills, ii) Northern plains as Brahmaputra plain, and iii) Deccan
132 plateau as Karbi Anglong (Dikshit and Dikshit 2014).
133 The state of Assam can be divided into five administrative levels as (i) Upper Assam, (ii) Lower
134 Assam, (iii) Central Assam, (iv) North Assam, and (v) Barak Valley (Figure 1). According to
135 the 2011 census, the population growth rate is 16.93%, and districts like Sonitpur, Cachar,
136 Dhubri, Barpeta, Kamprup, Darrang, and Nagaon have high population density (Census 2011).
137 The highest contribution to the economy of Assam is agricultural activities, and the majority
138 of the population is rural involved in the agricultural sector (Figure 1). The climate of Assam
139 is a tropical monsoon rainforest climate with heavy rainfall and high humidity. The summers
140 are warm (temperature 32°-38°) and mild winters (temperature 8°-20°). The region experiences
141 heavy annual rain ranging from 1500 to 3750 mm both in the plain and mountain areas due to
142 the southwest monsoon, mainly in May to September, which causes floods (Chaliha et al.
143 2012).

144 **Figure 1**

145 Two river systems, Brahmaputra and Barak, are present in the Assam region. In Assam, the
146 Brahmaputra valley is bounded by Himalayan mountains, Patkai hill ranges, and plains of
147 Bangladesh in the northern, eastern, and southern parts, respectively (Deka et al. 2012). Due to
148 the high flood frequency of the Brahmaputra river, it is known as "the river of sorrow" in
149 Assam (Dhar and Nandargi 2004). The tributaries of Brahmaputra River are rainfed in nature

and classified as north bank tributaries namely Subansiri, Ronganadi, Dikrong, Buroi, Borgong, Jiabharali, Dhansiri (North) Puthimari, Manas, Beki, Aie, Sonkosh and south bank tributaries namely Noadehing, Buridehing, Desang, Dikhow, Bhogdoi, Dhansiri (South), Kopilli, Kulsi, Krishnai, Dhudhnoi, Jinjiran (Jain et al. 2007).

The Barak River system is present in the southern part of Assam, forming Barak valley, and it finally drains into Bangladesh (Deka et al. 2012). The main tributaries of Barak rivers are Katakhal, Jiri, Chiri, Modhura, Longai, Sonai, Rukni, and Singla, mainly rainfed tributaries and are highly vulnerable to flooding during rainfall periods (Jain et al. 2007).

Assam experiences flood every year, causing inundation of villages, damages to croplands, loss of livelihood, lakhs of families becoming homeless and affecting the entire NER due to connectivity disruption (Sharma et al. 2018). According to Rashtriya Barh Ayog (RBA), the total flood-prone area of Assam is 31.05 Lakh Hectares which constitute about 40 % of the total area of Assam and 9.40% of the total flood-prone area of India. Hence, flood risk mapping is essential for Assam to facilitate effective flood management practice and planning.

3. Methodology

The methodology can be divided into the following sections: (1) preparation of spatial geodatabase for flood hazard and vulnerability indicator, (2) application of MCDA-AHP for weightage assignment of the indicators, (3) quantification of flood hazard index (FHI), flood vulnerability index (FVI), and flood risk index (FRI) at the regional and administrative level and (4) validation of flood hazard and risk models.

3.1. Flood hazard indicators

Flood hazard indicators are selected based on literature review, and corresponding thematic layers are generated using GIS.

3.1.1. Elevation and slope

174 The criteria of elevation and surface slope can delineate the regions having different levels of
175 flood hazard. The downstream areas at lower elevation and flat slopes are more prone to
176 flooding than those with high elevation and steep slopes. The elevation and slope layers are
177 created from SRTM 1 arc-second (30m resolution) DEM. The void data was filled, mosaiced,
178 and extracted by mask with the help of spatial analyst tool, and the attributes were calculated
179 using a zonal statistics tool (Souissi et al. 2020).

180 *3.1.2. Drainage density*

181 Drainage density can be defined as the length of river channels per unit area of the basin, and
182 it represents flow accumulation pathways (Arora et al. 2019). The drainage network map of the
183 study area is generated from DEM data using the hydrology tools, and drainage density is
184 calculated by the line density tool in GIS (Vignesh et al. 2021).

185 *3.1.3. Distance to river*

186 Proximity to the river channels plays a critical role in flood hazard modeling. During the river's
187 overflow, the river's volume will exceed its drainage capacity, and the water depth in the areas
188 located near the riverbed will increase significantly. The flood inundation will not impact only
189 the nearest river location, but the waterlogging and risk of flood will expand to the surroundings
190 (Chakraborty and Mukhopadhyay 2019). A raster layer is created using the Euclidean distance
191 tool in GIS (Toosi et al. 2019).

192 *3.1.4. Distance to embankment breach locations*

193 Embankments are man-made structures used as flood mitigation measures to protect the
194 settlements around the riverbanks. Breaching of the embankment can cause potential flood
195 damage (Hazarika et al. 2018). The locations of embankment breaches are identified by the
196 historical flood records, literature review, and Assam State Disaster Management Authority

197 (ASDMA) reports. The coordinates of the locations are extracted from Google Earth and using
198 the Euclidean distance tool, a raster layer is prepared (Chakraborty and Mukhopadhyay 2019).

199 *3.1.5. Soil texture*

200 Soil texture is a significant flood hazard indicator as the regional internal drainage system,
201 surface runoff, and moisture contents are highly influenced by the prevailing soil texture (Arora
202 et al. 2018). The soil data is obtained from the Food and Agriculture Organization of the United
203 Nations Educational, Scientific and Cultural Organization (FAO-UNESCO) and classified into
204 five soil classes (a) sandy clay loam, (b) loam, (c) clay loam, (d) clay, and (e) sandy loam
205 (Pareta 2021).

206 *3.1.6. Geology*

207 Geology controls the hydraulic properties of the bedrock of a region. The bedrock with
208 fractured, high porosity and permeability enhances the infiltration rate of rainwater, thus
209 minimizing the risk of flood. The geology map is extracted from the National Geologic Map
210 Database (NGMDB), USGS, and classified into four classes as (a) sedimentary, (b)
211 metamorphic, (c) Precambrian, and (d) Paleozoic rocks (Bhandari et al. 1973).

212 *3.1.7. Geomorphology*

213 Floods give rise to different landforms like erosional and depositional landforms. The
214 geomorphological data is obtained from the Bhukosh-Geological Survey of India (GSI)
215 (https://bhukosh.gsi.gov.in/Bhukosh/MapViewer.aspx), and classified into (a) structural hills,
216 (b) denudational hills, (c) alluvial plains, (d) pediplain, and (e) floodplain (Vignesh et al. 2021).

217 *3.1.8. Topographic Wetness Index (TWI)*

218 TWI is used to assess the effect of topography on the hydrological process of a watershed and
219 allows delineation of flood inundated areas (Pourali et al. 2016). For *TWI*, slope and flow

accumulation layers are generated from DEM data. *TWI* is calculated by the equation (1) given by Beven and Kirkby (1979)

$$TWI = \ln\left(\frac{A}{\tan\beta}\right) \quad (1)$$

where A represents source contributing area and tan β is ground surface slope. Higher *TWI* indicates the area is more prone to flood, and lower value denotes the steepest slope and less flood-prone regions (Arora et al. 2019).

Figure 2

3.1.9. Rainfall Erosivity Factor (REF)

Soil erosion is a significant problem during floods, and its rate depends on rainfall intensity. With the help of REF, the impact of rainfall intensity on soil erosion can be quantified. REF is calculated by equation (2) developed by Singh et al. (1981) using the average daily rainfall data of 21 years from 2000 to 2020 (Pathan and Sil 2020).

$$R = 79 + 0.363 \times P \quad (2)$$

Here, R and P represent rainfall erosivity factors (MJ mm ha^{-1} hr^{-1} $year^{-1}$) and mean annual precipitation (mm), respectively.

3.1.10. Rainfall intensity

Rainfall intensity is a crucial parameter that induces the occurrence of floods. Rainfall data from 2000 to 2020 are collected from Indian Meteorological Department (IMD), and rainfall intensity is determined for 114 grid points using equation (3). Rainfall intensity map is developed using Modified Fournier Index (*MFI*) approach and interpolated by Inverse Distance Weighting (IDW) interpolation in GIS (Toosi et al. 2019).

241 $$MFI = \sum_{i=1}^{12} \frac{P_i^2}{P} \quad (3)$$

242 P_i and P are the mean monthly and annual precipitation (mm), respectively.

243 *3.1.11. Runoff coefficient*

244 In the present study, rainfall-runoff modeling is performed using the National Resources
245 Conservation Services-Curve Number (NRCS-CN) method to estimate the surface runoff
246 coefficient for 33 basins in the study area (Pathak et al. 2020). The required input datasets are
247 DEM, soil data, land use land cover (LULC), and rainfall data of the study area (Toosi et al.
248 2019).

249 The runoff coefficient (*RC*) is calculated by the rational method using equation (4)

250 $$RC = \frac{Q}{P} \quad (4)$$

251 The surface runoff of an area is given by equations (5) to (10)

252 $$P = I + F + Q \quad (5)$$

253 *P, F,* and *Q* signify precipitation, initial abstraction, actual retention, and direct runoff,
254 respectively.

255 The ratio of actual rainfall retention to the potential maximum retention *S* is equal to the ratio
256 of direct runoff to rainfall minus initial abstraction.

257 $$\frac{(P-I-Q)}{S} = \frac{Q}{(P-I)} \quad (6)$$

258 $$Q = \frac{(P-I)^2}{(P-I+S)} \quad (7)$$

259 $$I = \lambda S$$

260 (8)

$$Q = \frac{(P - \lambda S)^2}{P + (1 - \lambda)S} \quad \text{For } P > \lambda S \tag{9}$$

$$Q = 0 \quad \text{For } P \leq \lambda S \tag{10}$$

λ is initial abstraction coefficient (ranging from 0 to infinity); in general, λ = 0.2 is recommended.

The value of S for the derived curve number (CN) of the basin can be calculated by equation (11).

$$S = \frac{25400}{CN} - 254 \tag{11}$$

CN is a dimensionless parameter ranging between 0 to 100 (USAD 2004; Al-Ghobari et al. 2020).

CN_i values are determined for each sub-basin, with different land uses, soil types, and areas (A_i). The final composite curve number (CN_w) is estimated by weighting the resulting CN values in equation (12).

$$CN_w = \frac{CN_i \times A_i}{A} \tag{12}$$

3.2. Flood Vulnerability indicators

Datasets for flood vulnerability indicators were collected from different global, national, regional platforms and processed in the GIS environment for further analysis.

3.2.1. *Population density*

Population density data are obtained from the Census 2011 (Census 2011). It directly relates to vulnerability because more people will be exposed to hazardous events in an area with a high population density (Chakraborty and Mukhopadhyay 2019).

3.2.2. Vulnerable population

The vulnerable population of the study area comprises females, children, and the old-aged population due to their low resilient capacity and high dependency. From the Census 2011, the

284 data are extracted to estimate the spatial distribution of the vulnerable population (Sharma et
285 al. 2018).
286 *3.2.3. Employment rate*
287 The economic status of the population highly influences the coping capacity of an area. A well-
288 defined income source of a community improves the living standard and increases the
289 community's coping capacity. The employment status for the Assam region is acquired from
290 Census 2011 (Agrawal et al. 2021).
291 *3.2.4. Literacy rate*
292 The literacy rate of an area is directly related to a community's awareness about the hazard and
293 helps in the preparedness during the hazardous event. Here, the literacy rate of Assam is
294 obtained from Census 2011, and its thematic layer is generated (Sharma et al. 2018).
295 *3.2.5. Household with more than four family members*
296 The household size directly influences the vulnerability component. A smaller household will
297 be less vulnerable than a household with more family members. The data of households are
298 collected from Census 2011 (Agrawal et al. 2021).
299 *3.2.6. Dilapidated house*
300 The condition of building structures determines their coping capacity towards any disaster. If
301 the building, mainly a residential building, is dilapidated, its vulnerability will increase. From
302 the Census 2011, data regarding the dilapidated houses are obtained (Agrawal et al. 2021).
303 **Figure 3**
304 *3.2.7. Building density*
305 Building density is considered an essential indicator for infrastructure vulnerability assessment,
306 and it is positively correlated with the vulnerability index. For the present study, building
307 density is calculated using the data obtained from the Census 2011 (Agrawal et al. 2021).
308 *3.2.8. Distance to roads*

A well-connected and maintained transportation system is one of the essential infrastructure components of a region. Road connectivity plays a critical role in relief and rescue operations during an emergency. Those settlements nearer to the roads are less vulnerable as they can be evacuated or rescued faster than the population residing in the remote areas (Hazarika et al. 2018). With the help of OpenStreetMap, major and minor roads are extracted and digitized in GIS. A raster dataset is generated by the Euclidean distance tool in GIS (Pareta 2021).

3.2.9. Distance to hospital

Proximity to hospitals and healthcare centers will facilitate emergency rescue operations and post-disaster health management activities. The locations of hospitals are obtained from the Department of Health & Family Welfare, Government of Assam. Coordinates of 624 government hospitals are extracted from Google Earth, and distance from hospitals is calculated using the Euclidean distance tool in GIS (Chakraborty and Mukhopadhyay 2019; Toosi et al. 2019).

3.2.10. Distance to stream confluence

The areas near the stream confluence are more prone to flood inundation because during the flood at the confluence point, the channel tends to carry combined discharge and load of two or more upstream tributaries (Chakraborty and Mukhopadhyay 2019). From the drainage network layer of the study area, confluence points are identified, and the distance from the confluence point is determined using the Euclidean distance tool in GIS (Arora et al. 2019).

3.2.11. Flow accumulation

Flow accumulation is the flow concentration, and it is directly related to flood vulnerability (Vojtek and Vojteková 2019). It is lower upstream but higher downstream as many tributaries join the main channel downstream. For the present study, flow accumulation raster is prepared by 30m resolution of DEM data using hydrology tool in GIS.

333 *3.2.12. Landuse land cover (LULC)*

334 LULC governs the relationship between different hydrological parameters like runoff,
335 infiltration, and rainfall abstraction (Toosi et al. 2019). The urban and pasture land increase the
336 overflow of water, whereas forest and dense natural vegetation increase water infiltration and
337 abstractions. The land use land cover map with ten LULC classes for the study area is derived
338 from Sentinel -2 imagery (10 m resolution) by ESRI (Kontgis et al. 2021). The map is further
339 reclassified into five categories (a) water, (b) built-up area, (c) agricultural land, (d) natural
340 vegetation, and (e) bare land and validated by calculating the kappa coefficient (Vignesh et al.
341 2021).

342 The accuracy of the LULC map is checked by overall accuracy ($A_{OVERALL}$) and Kappa (K)
343 statistics, User's and Producer's accuracy (A_{USER} and $A_{PRODUCER}$) using equations (13) to (16)
344 (Gibril et al. 2017; Hishe et al. 2020). The detailed error matrix was computed for each
345 classification image, as it allowed evaluation of A_{USER} and $A_{PRODUCER}$ for each of the
346 information classes included in our classification scheme (Table 1). For the present study,
347 Google Earth was used for the validation of classification with N=373 points.

348 $$K = \frac{N\sum_{i=1}^{r} m_{ii} - \sum_{i=1}^{r}(m_{i+})(m_{+i})}{N^2 - \sum_{i=1}^{r}(m_{i+})(m_{+i})} \quad (13)$$

349 $$A_{OVERALL} = \left(\frac{1}{N}\right)\sum_{i=1}^{r} n_{ii} \quad (14)$$

350 $$A_{PRODUCER} = \frac{n_{ii}}{n_{icolumm}} \quad (15)$$

351 $$A_{USER} = \frac{n_{ii}}{n_{irow}} \quad (16)$$

352 Where r denotes the number of rows, m_{ii} number of observations in row i and column i, m_{+i}
353 and m_{i+} are the marginal total of row (r) and column (i), respectively, n_{ii} are the number of
354 observations correctly classified.

355 **Table 1**

356 The value of overall accuracy and Kappa coefficient are 90.88% and 0.885, respectively. The
357 Kappa coefficient value close to 1 signifies that the classified image and reference image shows
358 perfect agreement, and hence the classification performed in the study is acceptable.
359 All the thematic layers of flood hazard and vulnerability indicators are resampled to a 30 m
360 raster layer to minimize the error (Chakraborty and Mukhopadhyay 2019). Jenks Natural
361 Breaks method is applied to classify flood hazard and vulnerability indicators, except for
362 distance from rivers, roads, stream confluence, hospitals, embankment breach location, LULC,
363 geology, geomorphology, and soil type (Toosi et al. 2019).

364 *3.3. Analytical Hierarchy Process (AHP) as Multi-Criteria Decision Analysis (MCDA)*
365 *technique*

366 The weightage to flood hazard and vulnerability indicators are assigned using Analytical
367 Hierarchy Process (AHP) as Multi-Criteria Decision Analysis (MCDA) technique. It is
368 considered a systematic, multi-objective, and reliable approach developed by Saaty (Saaty
369 2000, 2008). AHP decomposes a problem into a simple and subjective evaluated sub-problem
370 hierarchy (Saaty 2000). The indicators are weighted according to relative importance on a scale
371 from 1 to 9 (Saaty 2008). The steps of AHP are as follows:

372 Step 1. Decompose the complex unstructured problem into a hierarchy of goals, criteria, and
373 indicators.
374 Step 2. Make a pairwise comparison of the indicators based on a qualitative scale (Table 2).

375 Step 3. Construct a square matrix of n x n where diagonal elements of the matrix are 1. If the
376 indicator in the i^{th} row of the matrix is more important than the indicator in the j^{th} column, then
377 the element (i, j) will be assigned a value greater than 1, and the element (j, i) will be its
378 reciprocal.

379 **Table 2**

380 **Table 3**

381 Step 4. The weights of the pairwise comparison matrix are normalized by the eigenvector
382 method using the equations (17) to (18).

383 $$X_{ij} = \frac{C_{ij}}{\sum_{i=1}^{n} C_{ij}} \quad (17)$$

384 $$V_{ij} = \frac{\sum_{j=1}^{n} X_{ij}}{n} \quad (18)$$

385 where C_{ij} is the indicator value in the pairwise comparison matrix, X_{ij} is the normalized score,
386 and V_{ij} is the priority vector representing the indicators' weight (W_{ind}).
387 Finally, the assigned normalized weights are tested for consistency ratio (*CR*) using equation
388 (19), where *CR* must be less than 0.1 and consistency index (*CI*) is calculated by equation (20).

389 $$CR = \frac{CI}{RI} \quad (19)$$

390 $$CI = \frac{\lambda \max - n}{n - 1} \quad (20)$$

391 λ_{max}, *RI* (Table 3), and *n* are principal eigenvector, random index, and the number of indicators,
392 respectively.

393 *3.4. Flood hazard, vulnerability, and risk index*

394 Flood hazard index (*FHI*), flood vulnerability index (*FVI*), and flood risk index (*FRI*) are
395 calculated in GIS using a raster calculator by equations (21) to (23). The index scores are

normalized and converted into a raster of grid size 30 m × 30 m to minimize error (Chakraborty and Mukhopadhyay 2019).

$$FHI = (W_{ELV} \times ELV) + (W_{Sl} \times Sl) + (W_{Dd} \times Dd) + (W_{Dr} \times Dr) + (W_{De} \times De) + (W_{St} \times St) + (W_{Geo} \times Geo) + (W_{Gm} \times Gm) + (W_{TWI} \times TWI) + (W_{MFI} \times MFI) + (W_{REF} \times REF) + (W_{RC} \times RC) \quad (21)$$

$$FVI = (W_{PD} \times PD) + (W_{VP} \times VP) + (W_{Emp} \times Emp) + (W_{LR} \times LR) + (W_{HH4} \times HH4) + (W_{DPH} \times DPH) + (W_{BD} \times BD) + (W_{DRd} \times DRd) + (W_{DH} \times DH) + (W_{Dc} \times Dc) + (W_{FA} \times FA) + (W_{LULC} \times LULC) \quad (22)$$

Here, $W_{indicator}$ is the weight of respective indicators.

$$FRI = FHI \times FVI \quad (23)$$

All the indices are classified into five classes: very low, low, moderate, high, and very high.

3.5. Flood hazard map validation

To validate the hazard map 478 historical flood location points are selected and used for the performance analysis based on the accuracy assessment of flood classification. The confusion matrix or error matrix is suitable to validate the accuracy (Arora et al. 2019; Cabrera and Lee 2019). Several parameters like overall accuracy (OA), true positive rate (PR_{TRUE}), false positive rate (PR_{FALSE}), true negative rate (NR_{TRUE}), and false-negative rate (NR_{FALSE}) are calculated using the equations (24) to (28):

$$OA = \frac{P_{TRUE} + N_{TRUE}}{P + N} = \frac{P_{TRUE} + N_{TRUE}}{P_{TRUE} + N_{TRUE} + P_{FALSE} + N_{FALSE}} \quad (24)$$

$$PR_{TRUE} = \frac{P_{TRUE}}{P_{TRUE} + N_{FALSE}} \quad (25)$$

$$NR_{TRUE} = \frac{N_{TRUE}}{N_{TRUE} + P_{FALSE}} \quad (26)$$

$$PR_{FALSE} = \frac{P_{FALSE}}{P_{FALSE} + N_{FALSE}} = 1 - NR_{TRUE} \quad (27)$$

$$NR_{FALSE} = \frac{N_{FALSE}}{N_{FALSE} + P_{TRUE}} = 1 - PR_{TRUE} \quad (28)$$

where P, N, P_{TRUE}, N_{TRUE}, P_{FALSE}, and N_{FALSE} denote positive, negative, true positive, true negative, false positive, and false negative, respectively.

For the 478 points, elevations are extracted by using GIS tools. The elevation for the points ranged between 5 m to 135 m. The points are interpolated by the Kriging interpolation method and identified that points belonging to this elevation range are flood-prone areas.

3.6. Flood risk map validation

Due to a lack of data on flood depths, storm discharge at micro levels, the validation of the result was based on historical flood events and flood-prone areas reported by Disaster Management authorities at state and district levels. A total of 1263 inundation-prone settlements in the study area are identified and converted as georectified points in the GIS environment. From the settlement layer, a set of points are generated for very low to very high flood risk with the help of a spatial statistics tool. To validate the flood risk model (FRM), indirect methods of relative mean error (*RME*) and root of mean-square error (*RMSE*) are applied by considering observed locations (*OL*) for reported sites and predicted locations (*PL*) for modeled sites (Chakraborty and Mukhopadhyay 2019). The values of *RME, RMSE,* percentage of relative error (RE_i), and standard error (SE_i) for FRM are calculated using equations (29) to (32).

$$RME = \frac{1}{n}\sum REi \quad (29)$$

$$RE_i = \frac{(OL - PL) \times 100}{OL} \quad (30)$$

$$RMSE = \sqrt{\frac{1}{n}(\sum SE_i)} \quad (31)$$

436 $$SE_i = (OL - PL)^2 \quad (32)$$

437 ## 4. Results and discussion

438 ### *4.1. Spatial distribution of Flood hazard and vulnerability indicators*

439 The extent of flood hazard and vulnerability depends on topographical, geological, drainage
440 characteristics, hydrological, meteorological, demographical conditions of the region (Toosi et
441 al. 2019; Pathak et al. 2020; Hazarika et al. 2018; Arora et al. 2019). The flood hazard and
442 vulnerability indicators are classified into different classes, and effective weights are assigned
443 according to their significance i.e., very low (1), low (2), moderate (3), high (4), and very high
444 (5) (Table 4 and 5) (Chakraborty and Mukhopadhyay 2019; Pathak et al. 2020).
445 A thematic layer of flood hazard indicators is generated in GIS (Figure 2(a)-2(l)). Lower,
446 North, Upper, and Barak valley of Assam are more flood-prone due to lower elevation, milder
447 slopes, lower TWI, sedimentary rock structure, and sandy clay loam soil texture. The drainage
448 density is relatively low in Northern Assam and high in the Lower, Upper, Central, and Barak
449 valleys of Assam, increasing its flood susceptibility (Vignesh et al. 2021). The Lower, Northern
450 and Upper Assam are highly susceptible to flood due to alluvial and flood plains. The REF
451 values in the Upper and Lower Assam ranges from very low to very high, very high to moderate
452 in the Barak valley, very low to low in Central, and moderate to very low in Northern Assam.
453 The rainfall intensity and runoff coefficient are moderate to very high for the Lower and Barak
454 valley of Assam.

455 **Table 4**

456 The vulnerability indicators can be grouped into four types of vulnerability (i) socioeconomic
457 (population density, vulnerable population, employment rate, literacy rate, and household with
458 more than 4 family members), (ii) infrastructure (building density, distance to roads, distance
459 to hospital, and several dilapidated houses), (iii) hydrological (flow accumulation and distance

460 to stream confluences) and (iv) land use (LULC) (Figure 3(a)-3(l)) (Sharma et al. 2018). The
461 population density ranges from very high to moderate for the Lower, Upper, and Barak valley
462 of Assam and low to very low in Central and Northern Assam.

463 **Table 5**

464 The vulnerable population is very high in some parts of the Lower, Central, Upper, and Barak
465 valley of Assam. The employment rate is very high in the upper region of Assam due to the
466 predominance of agricultural activities, and the majority of the population is self-employed.
467 Very high to moderate literacy rates are found in the Upper, Central, and Barak valley of Assam
468 and can be considered less vulnerable than those with low literacy rates. The housing condition
469 of Central and Upper Assam lies in very low to low vulnerable class along with moderate to
470 high building density. The LULC distribution is classified according to the flood hazard,
471 vulnerability, and risk index for the Assam region (Figure 4(a)-4(d)) (Toosi et al. 2019). The
472 indicators are dynamic and vary spatially and temporally (Souissi et al. 2020).

473 **Figure 4**

474 *4.2. Weightage assignment of indicators by AHP*

475 In the present study AHP, a multi-criteria decision analysis approach is used to generate flood
476 hazard index (FHI) and flood vulnerability index (FVI). The consistency ratio (CR) is 0.06 and
477 0.03 for flood hazard and vulnerability indicators, respectively, and the consistency index (CI)
478 is 0.09 for flood hazard and 0.04 for vulnerability indicators. Highly contributing factors for
479 flood hazard are rainfall intensity, slope, runoff coefficient, elevation, distance to rivers,
480 drainage density, and the least significant factors are erosivity factor, geomorphology, and
481 geology (Table 6) (Toosi et al. 2019).

482 **Table 6**

For flood vulnerability, highly contributing factors include population density, vulnerable population, land use landcover, whereas the least contributing factors are identified as employment and literacy rate (Table 7) (Chakraborty and Mukhopadhyay 2019). The weightage assigned to the indicators has a critical role in flood risk modeling (Arabameri et al. 2019; Chakrabortty et al. 2021).

Table 7

4.3. Mapping of FHI, FVI, and FRI

From the spatial distribution of the FHI, the influence of rainfall intensity, runoff coefficient, elevation, surface slope, distance to the river, and drainage density are highly significant (Toosi et al. 2019). The resulting flood hazard map shows a substantial relationship with the controlling factors and FHI values. Areas with alluvial plains fall under very high to moderate FHI, while regions with structural and denudational hills have very low to low flood hazard zonation (Vignesh et al. 2021). Upper and lower Assam have high TWI, and it comes under very high to high flood hazard zone. The Lower, Upper, and Barak valleys of Assam have very high FHI and low to very low FHI values observed for the Central Assam (Figure 5a). More than 70% of the total area lies in the moderate to very high FHI class (Figure 5d).

In the present study, significant weightage is given to demographic, land use landcover infrastructure, and hydrological indicators as vulnerability indicators. The FVI ranges from low to very low for Central and Upper Assam, high to very high for Lower Assam, moderate to low for Northern Assam, and low to very high for the Barak valley. A large proportion of the area is in a very high vulnerable zone located along West Bengal, Meghalaya, and Indo-Bangladesh border. These areas have very high to moderate population density, a very high percentage of the vulnerable population, low literacy and employment rate, and high building density (Chakraborty and Mukhopadhyay 2019). About 57.37% of the total areas have moderate to high FVI (Figure 5d). Very high to moderate FVI are observed for Lower and Barak valley of

508 Assam. For Upper and Northern Assam, moderate to very low FVI values are identified, and a
509 large part of Central Assam shows very low flood vulnerability (Figure 5b).

510 **Figure 5**

511 The FHI and FVI profiles of Assam are different because flood hazards represent real and
512 existing physical elements that alter gradually, and the more dynamic indicators determine
513 flood vulnerability (Sharma et al 2018).

514 The spatial distribution of FRI shows that both FHI and FVI contribute significantly to the
515 generation of FRI, but their influences differ in many parts of the study area. Northern Assam
516 has moderate to high FHI, and moderate to low FVI and FRI classes. For Upper Assam, the
517 FHI ranges from moderate to very high, FVI and FRI range from very low to moderate. Barak
518 valley has moderate to very high FHI values, low to high FVI and FRI classes. Lower Assam
519 falls in the moderate to a very high flood risk category, and Central Assam has low to very low
520 flood risk values. The spatial distribution of FRI indicates that flood vulnerability indicators
521 contribute more to the estimation of risk than the hazard indicators (Figure 5c). Moderate to
522 very high FRI is observed for more than 50% of the total study area (Figure 5d).

523 *4.4. Mapping of FHI, FVI, and FRI at the administrative level*

524 *4.4.1. Lower Assam*

525 In lower Assam, 90.29%, 86.03%, and 88.32% of the total study area fall under moderate to
526 very high FHI, FVI and FRI classes, respectively (Figure 6(p)-6(r)). Dhubri, Goalpara Barpeta,
527 Bongaigaon, and Chirang lie in high to very high FHI, FVI, and FRI zones. The FRI class for
528 Kokrajhar district ranges from high to low, with moderate FVI and very high FHI. Nalbari lies
529 in very high to high flood hazard zonation with moderate to high FVI resulting in high to
530 moderate FRI. The area of Kamrup and Baksa falls under very high to low FHI and FVI class
531 and high to low FRI class. The Kamprup metropolitan has very low to low FRI due to very low
532 FHI and moderate FVI (Figure 6(a)-6(c)).

533 *4.4.2. Upper Assam*

534 More than 55% of the total area of Upper Assam falls under high to very high FHI class, and
535 less than 10% lies in high to very high FVI and FRI class (Figure 6(p)-6(r)). All the seven
536 Upper Assam districts are in high FHI classes but moderate to very low FVI and FRI classes.
537 (Figure 6(d)-6(f)).

538 *4.4.3. Northern Assam*

539 The Darrang district lies under high to very high flood hazard, vulnerability, and risk class in
540 the Northern Assam. For Sonitpur, flood risk ranges from moderate to low due to lower flood
541 hazards and vulnerability. Udalgiri district lies in a very high FVI zone but has moderate to
542 low FHI, making it moderate towards flood susceptibility (Figure 6(g)-6(i)). The very high to
543 moderate FHI, FVI, and FRI classes contribute approximately 85%,71%, and 63% of the total
544 study area, respectively (Figure 6(p)-6(r)).

545 **Figure 6**

546 *4.4.4. Central Assam*

547 The districts of Morigaon and Nagaon lie in moderate flood hazard and risk zones, having very
548 high FVI due to high population density, low literacy rate, and agricultural lands and built-up
549 areas. Similar variations are observed for FHI, FVI, and FRI classes for Karbi Anglong and
550 Dima Hasao districts (Figure 6(j)-6(l)). About 70% of the total study area falls under very low
551 flood risk and vulnerability zone (Figure 6(q)-6(r)).

552 *4.4.5. Barak valley*

553 The FVI for the Karimganj district of Barak valley is very high, with moderate to very high
554 FHI and FRI classes. On the other hand, Hailakandi and Cachar districts lie in moderate to low
555 FVI and FRI classes with very high FHI (Figure 6(m)-6(o)). More than 60% of the study area
556 is observed under moderate to very high FRI zones (Figure 6r).

557 The detailed study on flood risk assessment is essential to create more comprehensive and
558 integrated flood risk management practices for flood-prone regions like Assam. Many studies
559 have considered MCDA to develop a flood risk model using hydrological, geological,
560 demographical, and LULC indicators (Armenakis et al. 2017; Chakrabortty et al. 2021). The
561 spatial distribution of the indicators has a critical impact on the variation of FHI, FVI, and FRI
562 at the regional and administrative levels. For FRI development, the main limitations are related
563 to the database, including soil, topography, meteorological, lithological, historical flood events,
564 etc (Sarmah et al. 2020; Souissi et al. 2020). In the flood hazard assessment, rainfall intensity
565 is given higher weightage, followed by slope and runoff coefficient (Toosi et al. 2019). Factors
566 like elevation, slope, distance to river, geomorphology, soil type drainage density are used by
567 many researchers for the flood hazard assessment of Assam and other areas (Kumar 2016;
568 Pathak et al. 2020; Pareta 2021). But factors like TWI, REF, and runoff coefficient are limited,
569 especially for Assam.
570 Similarly, for the FVI, more weightage is given to demographical indicators and LULC of the
571 study area. The weightage assignment of the flood and vulnerability indicators is not constant,
572 and it depends from region to region (Sarkar and Mondal 2020; Rashetnia and Jahanbani 2021).
573 The results obtained by integrating MCDA(AHP)-GIS for the flood risk assessment of Assam
574 will provide the urban planners, engineers, policymakers a reliable and efficient tool for
575 identifying flood-prone zones and making effective preparedness and mitigation strategies.

576 **5. Result validation**

577 *5.1. Flood hazard index map*

578 Based on 478 historical flood points, a resulting flood map was created by the interpolation
579 method in GIS software and overlaid with the flood hazard index map, obtained by applying
580 AHP. After performing the accuracy assessment by the confusion matrix or error matrix
581 method, the number of pixels that matched correctly (P_{TRUE}) and mistakenly (P_{FALSE}) are

582 calculated (Table 8). The estimated accuracy is 90.75%. Calculated PR_{TRUE}, NR_{TRUE}, PR_{FALSE},
583 and NR_{FALSE} values are 0.90, 0.92, 0.08, and 0.10, respectively.

584 **Table 8**

585 *5.2. Flood risk index map*

586 Relative mean error (RME) and root of mean-square error (RMSE) were applied to validate
587 the flood risk map of Assam, based on the selection of 1263 flood-prone locations. The model
588 accurately predicted 1089 locations and has an accuracy of 86.22%, the overall efficiency of
589 the model is found to be satisfactory, with RMSE equal to 0.105 and RME equal to 0.391. For
590 the districts like Barpeta, Chirang, Cachar, Lakhimpur, Nalbari, Morigaon, Tinsukia,
591 Karimganj, Golaghat, Jorhat, Udalguri, Naogaon, Sivasagar, Dima Hasao, Dhubri, Sonitpur,
592 Darrang, Dhemaji, Goalpara, Bongaigaon, Kokrajhar shows accuracy level between 85-96%
593 and district like Kamrup metropolitan, Kamrup rural, Baksa, Hailakandi, Dibrugarh, Karbi
594 Anglong have accuracy level ranging from 78-85%.

595 **6. Conclusion**

596 In the present study, the flood hazard, vulnerability, and risk maps of Assam at the regional
597 and administrative levels are developed by combining MCDA-AHP and GIS tools. The flood
598 hazard and vulnerability layer are created using different indicators, and AHP is applied to
599 assigned weightage to the indicator. The final flood risk map is obtained by integrating hazard
600 and vulnerability indices in GIS software and validated by confusion matrix, RME, and RMSE
601 based on historical flood events. The results show that more than 70% of the total area lies in
602 the moderate to very high FHI class, and it includes Lower, Upper, and Barak valley of Assam
603 have very high FHI. About 57.37% of the total areas have moderate to high FVI consisting of
604 the Lower and Barak valley of Assam, whereas the Central Assam shows very low flood
605 vulnerability. For more than 50% of the total study area, moderate to very high FRI are
606 observed in the Lower, Upper, and Barak valley of Assam. The FHI, FVI, and FRI indices

607 estimate the flood-prone areas of Assam and spatial variation of the indicators responsible for
608 flood occurrence. The districts like Dhubri, Goalpara Barpeta, Bongaigaon, Darrang,
609 Karimganj, and Chirang lie in high to very high FHI, FVI, and FRI zones. The study has
610 inherent limitations related to the database, including soil, topography, meteorological,
611 lithological, historical flood events, and weightage assignment. The results may provide the
612 local governing authorities and stakeholders with a comprehensive tool for flood risk
613 management. The methodology can be implemented in other locations to carry out a flood risk
614 assessment with more accurate and precise data sources using time and cost-effective GIS-
615 based tools.

616 **Data Availability Statement**

617 The authors confirm that the data supporting the findings of this study are available within the
618 article and some of the raw data were generated at our laboratory and derived data supporting
619 the findings of this study are available upon reasonable request.

620 **Declaration of Competing Interests**

621 The authors declare that they have no known competing financial interests or non-financial
622 interests or personal relationships that are directly or indirectly related to the work submitted
623 for publication that could have appeared to influence the work reported in this paper.

624 **References**

625
626 Agrawal N, Gupta L, Dixit J. 2021. Assessment of the Socioeconomic Vulnerability to Seismic
627 Hazards in the National Capital Region of India Using Factor Analysis. Sustainability.
628 13(17):9652.

629 Al-Ghobari H, Dewidar A, Alataway A. 2020. Estimation of surface water runoff for a semi-
630 arid area using RS and GIS-based SCS-CN method. Water. 12(7):1924.

631 Arabameri A, Rezaei K, Cerdà A, Conoscenti C, Kalantari Z. 2019. A comparison of statistical
632 methods and multi-criteria decision making to map flood hazard susceptibility in Northern
633 Iran. Sci Total Environ. 660:443-458.

634 Armenakis C, Du EX, Natesan S, Persad RA, Zhang Y. 2017. Flood risk assessment in urban
635 areas based on spatial analytics and social factors. Geosciences. 7(4):123.

636 Arora A, Pandey M, Siddiqui MA, Hong H, Mishra VN. 2019. Spatial flood susceptibility
637 prediction in Middle Ganga Plain: comparison of frequency ratio and Shannon's entropy
638 models. Geocarto Int. 1-32.

639 Beven KJ, Kirkby MJ. 1979. A physically based, variable contributing area model of basin
640 hydrology. Hydrol Sci J. 24(1):43-69.

641 Bhandari LL, Fuloria RC, Sastri VV. 1973. Stratigraphy of Assam Valley, India. AAPG
642 Bulletin. 57(4):642-654.

643 Borah SB, Sivasankar T, Ramya MNS, Raju PLN. 2018. Flood inundation mapping and
644 monitoring in Kaziranga National Park, Assam using Sentinel-1 SAR data. Environ
645 monitoring and Assess. 190(9):1-11.

646 Brito MMD, Evers M, Almoradie ADS. 2018. Participatory flood vulnerability assessment: a
647 multi-criteria approach. Hydrol Earth Syst Sci. 22(1):373-390.

648 Cabrera JS, Lee HS. 2019. Flood-prone area assessment using GIS-based multi-criteria
649 analysis: a case study in Davao Oriental, Philippines. Water. 11(11):2203.

650 Census. 2011. Population Census 2011. https://www.census2011.co.in/

651 Chakrabortty R, Chandra Pal S, Rezaie F, Arabameri A, Lee S, Roy P, Saha A, Chowdhuri I,
652 Moayedi H. 2021. Flash-flood hazard susceptibility mapping in Kangsabati River Basin,
653 India. Geocarto Int. 1-23.

654 Chakraborty S, Mukhopadhyay S. 2019. Assessing flood risk using analytical hierarchy
655 process (AHP) and geographical information system (GIS): application in Coochbehar
656 district of West Bengal, India. Nat Hazards. 99(1):247-274.
657 Chaliha S, Sengupta A, Sharma N, Ravindranath NH. 2012. Climate variability and farmer's
658 vulnerability in a flood-prone district of Assam. Int J Climate Change Strategies and
659 Manage. 4:179–200
660 Chen H, Ito Y, Sawamukai M, Tokunaga T. 2015. Flood hazard assessment in the Kujukuri
661 Plain of Chiba Prefecture, Japan, based on GIS and multicriteria decision analysis. Nat
662 Hazards. 78(1):05-120.
663 Choubin B, Moradi E, Golshan M, Adamowski J, Sajedi-Hosseini F, Mosavi A. 2019. An
664 ensemble prediction of flood susceptibility using multivariate discriminant analysis,
665 classification and regression trees, and support vector machines. Sci Total Environ.
666 651:2087-2096.
667 CRED. 2019. EM-DAT:The Int Disaster Database. Centre for Research on the Epidemiology
668 of Disasters.
669 Dandapat K, Panda GK. 2017. Flood vulnerability analysis and risk assessment using analytical
670 hierarchy process. Model Earth Syst Environ. 3(4):1627-1646.
671 Danso SY, Ma Y, Adjakloe YDA, Addo IY. 2020. Application of an Index-Based Approach
672 in Geospatial Techniques for the Mapping of Flood Hazard Areas: A Case of Cape Coast
673 Metropolis in Ghana. Water. 12(12):3483.
674 Deka RL, Mahanta C, Pathak H, Nath KK, Das S. 2013. Trends and fluctuations of rainfall
675 regime in the Brahmaputra and Barak basins of Assam, India. Theoretical and Appl
676 climatology. 114(1):61-71.

677 Dekongmen BW, Kabo-bah AT, Domfeh MK, Sunkari ED, Dile YT, Antwi EO, Gyimah RAA.
678 2021. Flood vulnerability assessment in the Accra Metropolis, southeastern Ghana. Appl
679 Water Sci. 11(7):1-10.
680 Dewan AM, Kumamoto T, Nishigaki M. 2006. Flood hazard delineation in greater Dhaka,
681 Bangladesh using an integrated GIS and remote sensing approach. Geocarto Int. 21(2):33-
682 38.
683 Dhar ON, Nandargi S. 2004. Rainfall distribution over the Arunachal Pradesh
684 Himalayas. Weather. 59(6):155-157.
685 Dikshit KR, Dikshit JK. 2014. Relief features of north-east India. In North-East India: Land,
686 People and Economy. Dordrecht: Springer ; p.91-125
687 FAO and ITPS. 2015. Main report: Status of the World's Soil Resources; Food and Agriculture
688 Organization of the United Nations and Intergovernmental Technical Panel on Soils,
689 Rome, Italy.
690 Gibril MBA, Bakar SA, Yao K, Idrees MO, Pradhan B. 2017. Fusion of RADARSAT-2 and
691 multispectral optical remote sensing data for LULC extraction in a tropical agricultural
692 area. Geocarto Int. 32(7):735-748.
693 Hazarika N, Barman D, Das AK, Sarma AK, Borah SB. 2018. Assessing and mapping flood
694 hazard, vulnerability and risk in the Upper Brahmaputra River valley using stakeholders'
695 knowledge and multicriteria evaluation (MCE). J Flood Risk Manage. 11:S700-S716.
696 Hishe S, Bewket W, Nyssen J, Lyimo J. 2020. Analysing past land use land cover change and
697 CA-Markov-based future modelling in the Middle Suluh Valley, Northern
698 Ethiopia. Geocarto Int. 35(3):225-255.
699 Jain SK, Agarwal PK, Singh VP. 2007. Brahmaputra and Barak Basin. In Hydrology and water
700 resources of India. Dordrecht: Springer; p. 419-472.

701 Khosravi K, Panahi M, Golkarian A, Keesstra SD, Saco PM, Bui DT, Lee S. 2020.
702 Convolutional neural network approach for spatial prediction of flood hazard at national
703 scale of Iran. J Hydrol. 591:125552.
704 Kontgis K, et al. "Global land use/land cover with Sentinel-2 and deep learning." IGARSS
705 2021-2021 IEEE Int Geoscience and Remote Sensing Symposium. IEEE, 2021.
706 Kumar R. 2016. Flood hazard assessment of 2014 floods in Sonawari sub-district of Bandipore
707 district (Jammu & Kashmir): An application of geoinformatics. Remote Sensing
708 Applications: Society and Environ. 4:188-203.
709 Lyu HM, Sun WJ, Shen SL, Arulrajah A. 2018. Flood risk assessment in metro systems of
710 mega-cities using a GIS-based modeling approach. Sci Total Environ. 626:1012-1025.
711 Majumder R, Bhunia GS, Patra P, Mandal AC, Ghosh D, Shit PK. 2019. Assessment of flood
712 hotspot at a village level using GIS-based spatial statistical techniques. Arab J
713 Geosci. 12(13):1-12.
714 Mishra K, Sinha R. 2020. Flood risk assessment in the Kosi megafan using multi-criteria
715 decision analysis: A hydro-geomorphic approach. Geomorphology. 350:106861.
716 Pareta K. 2021. Multi-Criteria Analysis (MCA) for Identification of Vulnerable Areas Along
717 Brahmaputra River in Assam and Their Field Assessment. J of Environ Protection and
718 Sustainable Development. 7(2):15-29.
719 Pathak S, Liu M, Jato-Espino D, Zevenbergen C. 2020. Social, economic and environmental
720 assessment of urban sub-catchment flood risks using a multi-criteria approach: A case
721 study in Mumbai City, India. J Hydrol. 591:125216.
722 Pathan SA, Sil BS. 2020. Prioritization of soil erosion prone areas in upper Brahmaputra River
723 Basin up to Majuli River Island. Geocarto Int. 1-19.

724 Pourali SH, Arrowsmith C, Chrisman N, Matkan AA, Mitchell D. 2016. Topography wetness
725 index application in flood-risk-based land use planning. Appl Spatial Analysis and
726 Policy. 9(1):39-54.

727 Rashetnia S, Jahanbani H. 2021. Flood vulnerability assessment using a fuzzy rule-based index
728 in Melbourne, Australia. Sustainable Water Resources Manage. 7(2):1-13.

729 Rong Y, Zhang T, Zheng Y, Hu C, Peng L, Feng P. 2020. Three-dimensional urban flood
730 inundation simulation based on digital aerial photogrammetry. J Hydrol. 584:124308.

731 Saaty TL. 2000. Fundamentals of decision making and priority theory with the analytic
732 hierarchy process (6). RWS publications.

733 Saaty TL. 2008. Decision making with the analytic hierarchy process. Int J Services Sci.
734 1(1):83-98.

735 Sadeghi-Pouya A, Nouri J, Mansouri N, Kia-Lashaki A. 2017. An indexing approach to assess
736 flood vulnerability in the western coastal cities of Mazandaran, Iran. Int J Disaster Risk
737 Reduct. 22:304-316.

738 Sarkar D, Mondal P. 2020. Flood vulnerability mapping using frequency ratio (FR) model: a
739 case study on Kulik river basin, Indo-Bangladesh Barind region. Appl Water Sci. 10(1):1-
740 13.

741 Sarmah T, Das S, Narendr A, Aithal BH. 2020. Assessing human vulnerability to urban flood
742 hazard using the analytic hierarchy process and geographic information system. Int J
743 Disaster Risk Reduct. 50:101659.

744 Shahiri Tabarestani E, Afzalimehr H. 2021. A comparative assessment of multi-criteria
745 decision analysis for flood susceptibility modelling. Geocarto Int. 1-24.

746 Sharma TPP, Zhang J, Koju UA, Zhang S, Bai Y, Suwal MK. 2019. Review of flood disaster
747 studies in Nepal: A remote sensing perspective. Int J Disaster Risk Reduct. 34:18-27.

748 Shivaprasad Sharma SV, Roy PS, Chakravarthi V, Srinivasa Rao G. 2018. Flood risk
749 assessment using multi-criteria analysis: a case study from Kopili River Basin, Assam,
750 India. Geomat Nat Hazards Risk. 9(1):79-93.

751 Singh G, Rambabu VV, Chandra S. 1981. Soil loss prediction research in India. Bulletin of
752 Central Soil and Water Conservation Research and Training Institute, T12/D9, Dehradun
753 Souissi D, Zouhri L, Hammami S, Msaddek MH, Zghibi A, Dlala M, 2020. GIS-based
754 MCDM–AHP modeling for flood susceptibility mapping of arid areas, southeastern
755 Tunisia. Geocarto Int. 35(9):991-1017.

756 Subrahmanyam VP. 1988. Hazards of floods and droughts in India. In Natural and man-made
757 hazards. Dordrecht: Springer; p. 337-356.
758 Toosi AS, Calbimonte GH, Nouri H, Alaghmand S. 2019. River basin-scale flood hazard
759 assessment using a modified multi-criteria decision analysis approach: A case study. J
760 Hydrol. 574:660-671.

761 USDA. 2004. Estimation of direct runoff from storm rainfall. National Engineering Hand- book
762 p. 79.
763 Vignesh KS, Anandakumar I, Ranjan R, Borah D. 2021. Flood vulnerability assessment using
764 an integrated approach of multi-criteria decision-making model and geospatial
765 techniques. Model Earth Syst Environ. 7(2):767-781.

766 Vojtek M, Vojteková J. 2019. Flood susceptibility mapping on a national scale in Slovakia
767 using the analytical hierarchy process. Water. 11(2):364.

768 Wang X, Xie, H. 2018. A review on applications of remote sensing and geographic information
769 systems (GIS) in water resources and flood risk management. Water. 10(5):608.

770 Zhang D, Shi X, Xu H, Jing Q, Pan X, Liu T, Wang H, Hou H. 2020. A GIS-based spatial
771 multi-index model for flood risk assessment in the Yangtze River Basin, China. Environ
772 Impact Assess Review. 83:106397.

773

774

775 **Table 1.** LULC classification and accuracy assessment

LULC CLASS	Water	Natural Vegetation	Agriculture	Built-up	Bare Land	**Total User**	**User's Accuracy (%)**	**Producer's Accuracy (%)**
Water	75	0	0	0	3	78	96.15	96.15
Natural Vegetation	0	65	6	0	3	74	87.84	91.55
Agriculture	0	6	60	4	3	73	82.19	88.24
Built-up	0	0	1	67	2	70	95.71	91.78
Barren Land	3	0	1	2	72	78	92.31	86.75
Total Producer	78	71	68	73	83	373		

776

777 **Table 2.** The scale of preference **(**Saaty 2008**)**

Degree of preference	**Scales**
Extremely	9
Very strongly to extremely	8
Very strongly	7
Strongly to very strongly	6
Strongly	5
Moderately to strongly	4
Moderately	3
Equally to moderately	2
Equally	1

778

779 **Table 3.** Value of Random Index (Saaty 2000)

n	3	4	5	6	7	8	9	10	11	12	13	14	15
RI	0.52	0.89	1.11	1.25	1.35	1.40	1.45	1.49	1.51	1.54	1.56	1.57	1.58

780

781 **Table 4.** Flood hazard indicators

Indicator	W_{ind}	Subclass	% of area	Effective weight (EF)	Normalized EF
Elevation (ELV)	0.10	5-135	73.69	5	0.33
		135.01-326	14.37	4	0.27
		326.01-600	6.11	3	0.20
		600.01-960	4.62	2	0.13
		960.01-1964	1.20	1	0.07
Slope (Sl)	0.14	0-3.07	48.83	5	0.33
		3.08-8.38	30.14	4	0.27
		8.39-15.92	12.46	3	0.20
		15.93-26.25	6.21	2	0.13
		26.26-71.21	2.35	1	0.07
Drainage Density (Dd)	0.09	0-0.26	30.28	1	0.07
		0.27-0.52	29.93	2	0.13
		0.53-0.79	23.32	3	0.20
		0.80-1.05	14.47	4	0.27
		1.06-1.31	2.00	5	0.33
Proximity to the river (Dr)	0.10	0-500	9.65	5	0.33
		501-1000	8.73	4	0.27
		1001-2000	15.44	3	0.20
		2001-4000	24.68	2	0.13
		>4000	41.49	1	0.07
Proximity to embankment breach locations (De)	0.05	0-500	0.09	5	0.33
		501-1000	0.27	4	0.27
		1001-2000	1.04	3	0.20
		2001-4000	3.74	2	0.13
		>4000	94.86	1	0.07
Soil texture (St)	0.06	Sandy clay loam	52.54	5	0.33
		Clay	3.72	4	0.27
		Sandy Loam	4.86	3	0.20
		Clay Loam	6.01	2	0.13
		Loam	32.87	1	0.07
Geology (Geo)	0.02	Metamorphic	0.60	2	0.20
		Paleozoic	1.17	1	0.10
		Precambrian	12.85	2	0.20
		Sedimentary	85.38	5	0.50

Geomorphology (Gm)	0.03	Alluvial plain	43.74	5	0.31
		Denudational hill	1.53	2	0.13
		Flood plain	25.75	5	0.31
		Pediplain	5.89	3	0.19
		Structural hill	24.89	1	0.06
Topographic wetness index (TWI)	0.05	2.35-8.06	65.30	2	0.20
		8.07-11.83	24.55	3	0.30
		11.84-28.33	10.14	5	0.50
Rainfall intensity (MFI)	0.19	148.45-254.22	28.68	1	0.07
		254.23-359.98	47.20	2	0.13
		359.99-465.75	14.89	3	0.20
		465.76-571.51	6.42	4	0.27
		571.52-677.28	2.81	5	0.33
Rainfall Erosivity Factor (REF)	0.03	419.02-639.71	23.64	1	0.07
		639.72-786.84	29.56	2	0.13
		786.85-941.32	25.47	3	0.20
		941.33-1114.20	14.39	4	0.27
		1114.21-1356.96	6.93	5	0.33
Runoff coefficient (RC)	0.12	0-0.04	30.87	1	0.07
		0.05-0.08	29.00	2	0.13
		0.09-0.13	26.63	3	0.20
		0.14-0.20	10.09	4	0.27
		0.21-30	3.40	5	0.33

782

783 **Table 5.** Flood vulnerability indicators

Indicator	W_{ind}	Sub class	% of area	Effective weight (EF)	Normalized EF
Population density (PD)	0.21	43.65-91.79	19.54	1	0.07
		91.80-364.22	27.27	2	0.13
		364.23-530.01	31.53	3	0.20
		530.02-743.15	20.65	4	0.27
		743.16-1574.76	1.02	5	0.33
Vulnerable population (VP)	0.19	59.23-65.34	1.03	3	0.14
		65.35-69.34	38.03	4	0.19
		69.35-70.44	28.97	4	0.19
		70.45-71.19	10.01	5	0.24
		71.20-73.48	21.97	5	0.24
Employment rate (Emp)	0.03	32.49-33.17	6.91	5	0.33
		33.18-36.68	22.68	4	0.27
		36.69-40.21	33	3	0.20
		40.22-42.81	26.06	2	0.13
		42.82-46.17	11.34	1	0.07
Literacy rate (LR)	0.03	47.32-53.90	9.99	5	0.33
		53.91-58.75	32.56	4	0.27

		58.76-61.79	17.91	3	0.20
		61.80-70.68	34.9	2	0.13
		70.69-79.84	4.63	1	0.07
Household with more than 4 family members (HH4)	0.06	64.72-68.32	7.53	3	0.14
		68.33-71.83	12.81	4	0.19
		71.84-75.57	39.4	4	0.19
		75.58-77.67	15.55	5	0.24
		77.68-81.83	24.7	5	0.24
Dilapidated house (DPH)	0.05	4.03-5.85	25.39	1	0.07
		5.86-7.46	11.3	2	0.13
		7.47-11.06	29.87	3	0.20
		11.07-14.12	23.26	4	0.27
		14.13-17.59	10.17	5	0.33
Building density (BD)	0.06	8.61-17.05	19.54	1	0.07
		17.06-85.78	20.53	2	0.13
		85.79-118.90	36.57	3	0.20
		118.91-149.74	18.82	4	0.27
		149.75-368.11	4.55	5	0.33
Proximity to roads (DRd)	0.05	0-500	9.72	1	0.07
		501-1000	11.2	2	0.13
		1001-2000	16.19	3	0.20
		2001-4000	22.67	4	0.27
		>4000	40.22	5	0.33
Proximity to hospital (DH)	0.04	0-500	0.10	1	0.07
		501-1000	0.29	2	0.13
		1001-2000	1.14	3	0.20
		2001-4000	4.37	4	0.27
		>4000	94.10	5	0.33
Distance to stream confluence (Dc)	0.07	0-500	0.07	5	0.33
		501-1000	0.20	4	0.27
		1001-2000	0.78	3	0.20
		2001-4000	3.11	2	0.13
		>4000	95.85	1	0.07
Flow accumulation (FA)	0.07	0-1000	97.77	1	0.07
		1001-2000	0.61	2	0.13
		2001-5000	0.56	3	0.20
		5001-12000	0.36	4	0.27
		>12000	0.70	5	0.33
Land use land cover (LULC)	0.14	Water	4.38	5	0.33
		Natural vegetation	43.74	2	0.13
		Agricultural land	34.10	3	0.20
		Builtup area	13.17	4	0.27
		Bare land	4.62	1	0.07

784

785

786 **Table 6.** Pair-wise comparison for flood hazard indicators

Indicators	MFI	Sl	ELV	Dr	Dd	St	REF	TWI	De	Gm	RC	Geo	W_{ind}
MFI	1	3	3	3	3	4	5	3	4	4	1	4	0.19
Sl		1	3	2	2	4	5	3	4	3	1	5	0.15
ELV			1	2	1	3	4	3	3	3	0.33	5	0.10
Dr				1	2	3	4	3	2	3	1	4	0.10
Dd					1	3	4	3	2	3	1	4	0.09
St						1	4	2	2	2	0.50	2	0.06
REF							1	2	1	1	0.20	2	0.03
TWI								1	1	2	1	2	0.05
De									1	3	0.33	4	0.05
Gm										1	0.33	3	0.03
RC											1	4	0.12
Geo												1	0.02

787

788 **Table 7.** Pair-wise comparison for flood vulnerability indicators

Indicators	PD	VP	LULC	Dc	FA	BD	HH4	DRd	DPH	DH	LR	Emp	W_{ind}
PD	1	1	4	4	4	3	3	4	4	5	4	4	0.21
VP		1	3	3	3	3	3	4	4	5	4	4	0.19
LULC			1	3	4	3	3	3	3	4	4	3	0.14
Dc				1	1	2	2	2	2	1	2	2	0.07
FA					1	1	1	2	2	3	2	2	0.07
BD						1	1	1	2	2	2	2	0.06
HH4							1	1	2	2	2	2	0.06
DRd								1	1	2	1	1	0.05
DPH									1	2	2	2	0.05
DH										1	2	2	0.04
LR											1	1	0.03
Emp												1	0.03

789

790 **Table 8.** Confusion matrix for flood hazard

	Predicted		
Observed	Non-Flood	Flood	Total
Non-Flood	P_{TRUE}	N_{FALSE}	Positive
Flood	P_{FALSE}	N_{TRUE}	Negative
Non-Flood	88878692	10153760	99032452
Flood	5777206	67551350	73328556

791

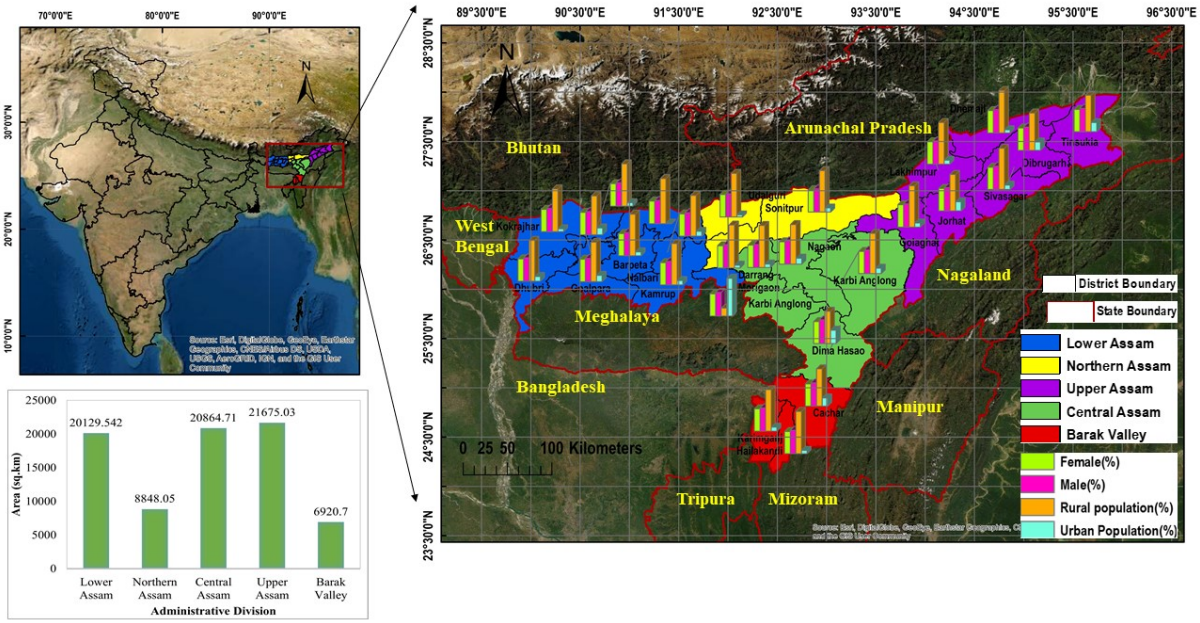

Figure 1. Map of the study area

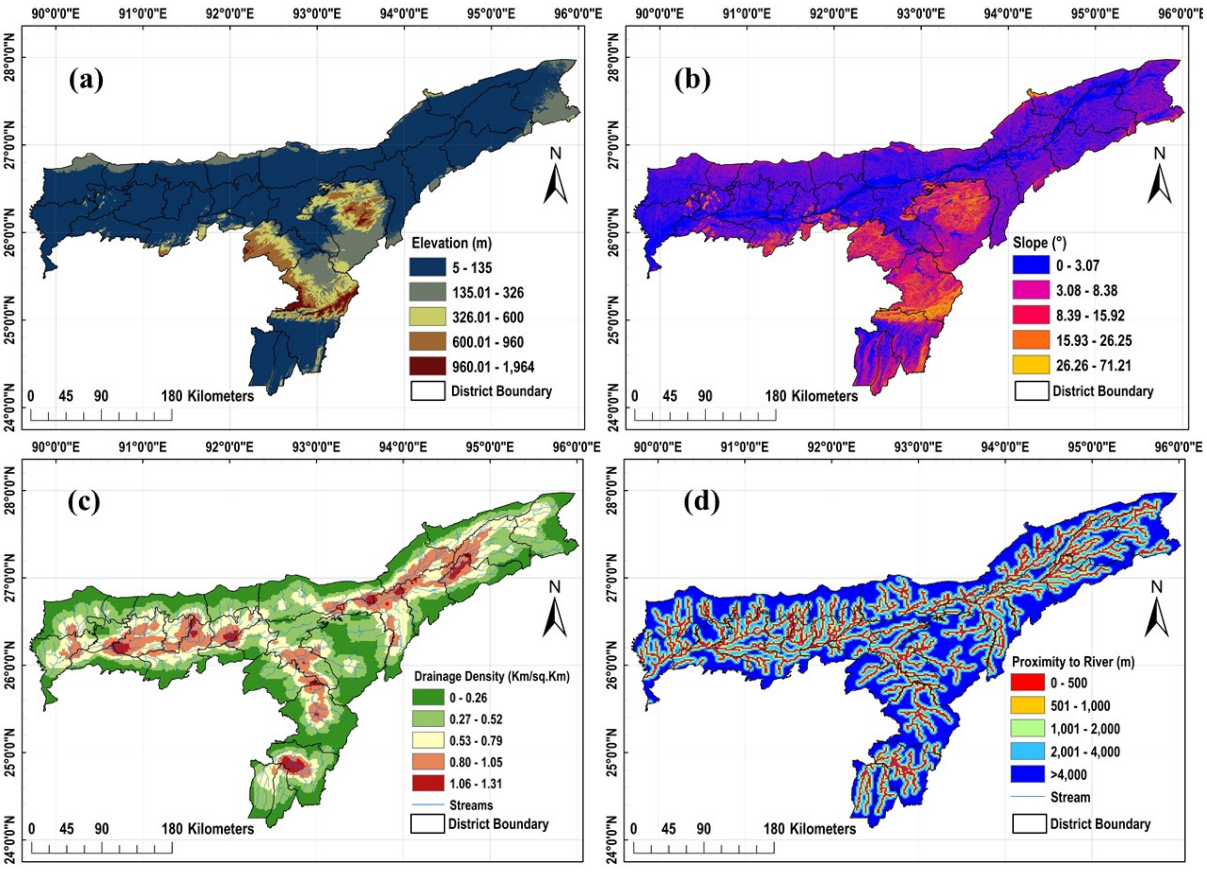

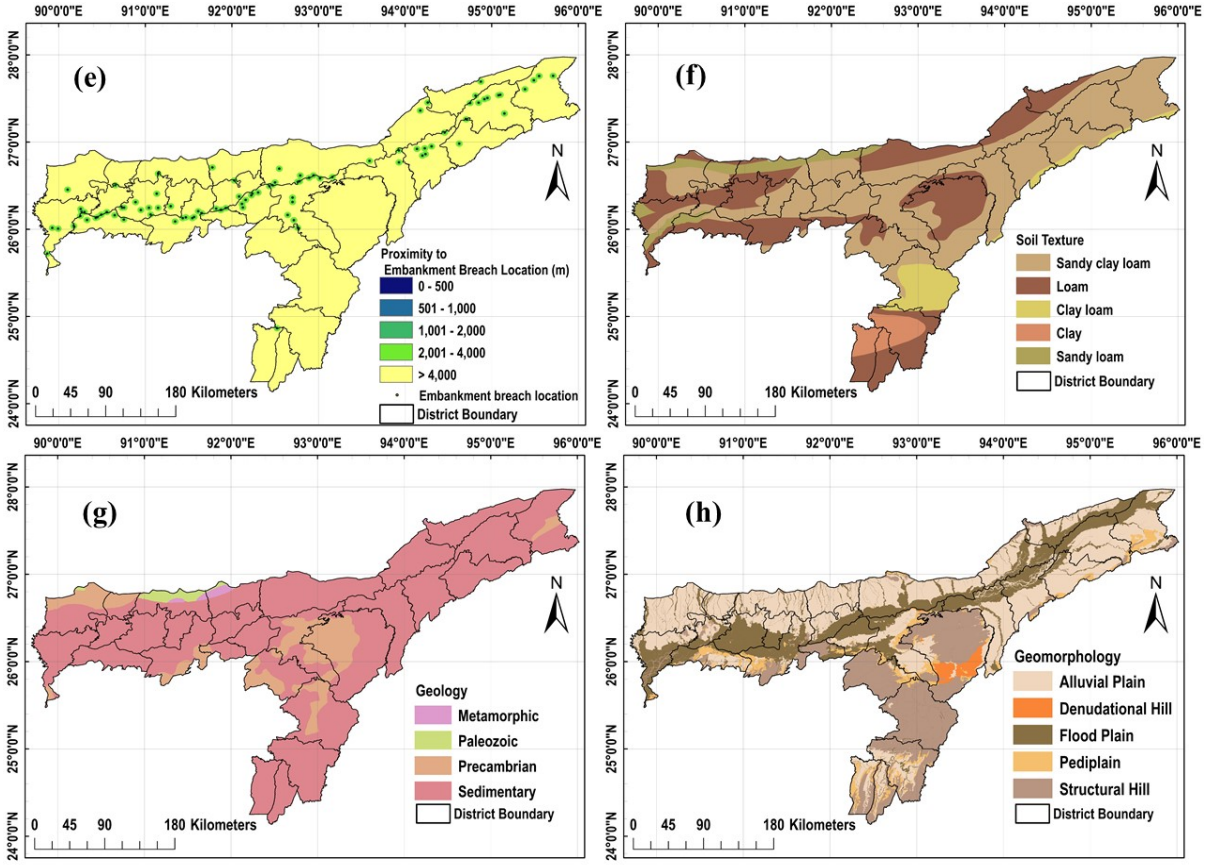

796

797

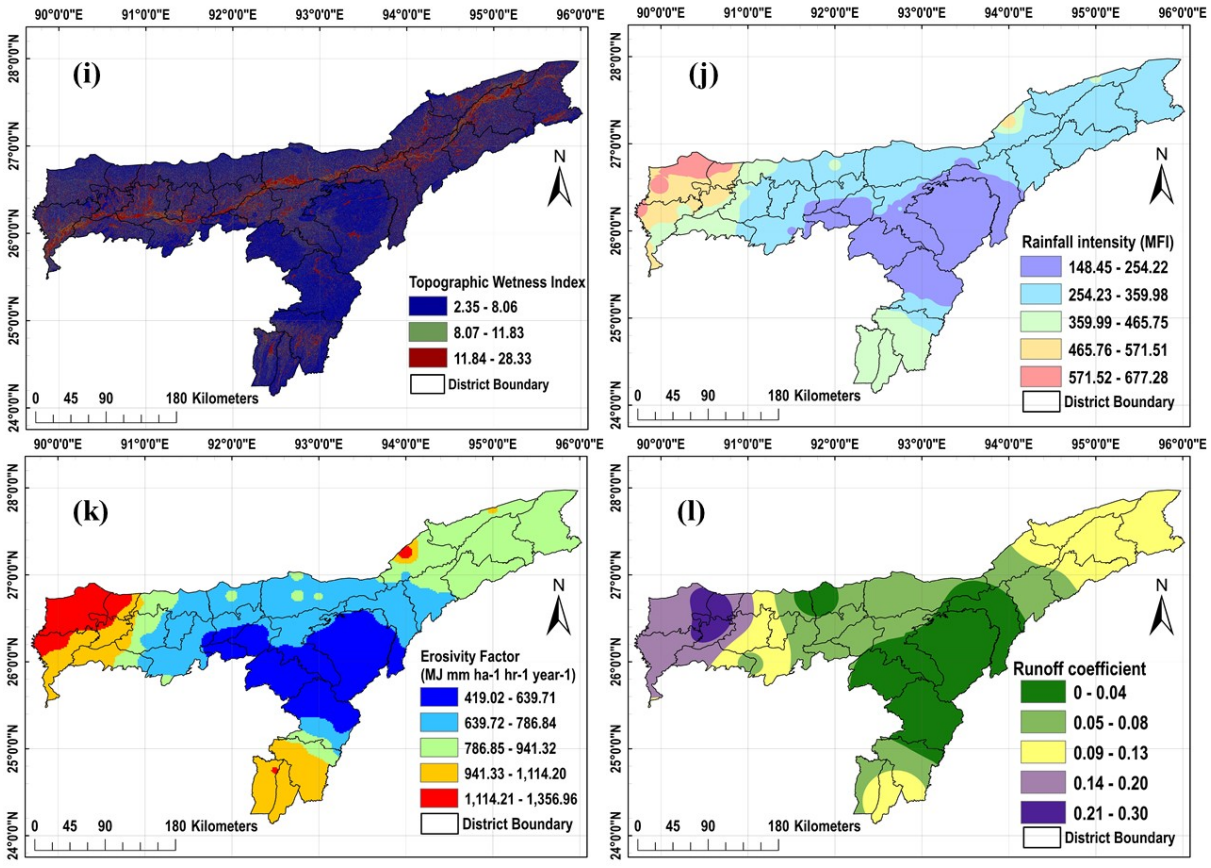

798

799

Figure 2. Flood hazard indicators (a) to (l) indicate elevation; slope; drainage density; proximity to the river; proximity to embankment; soil texture; geology; geomorphology; TWI; Rainfall intensity; erosivity factor; and runoff coefficient.

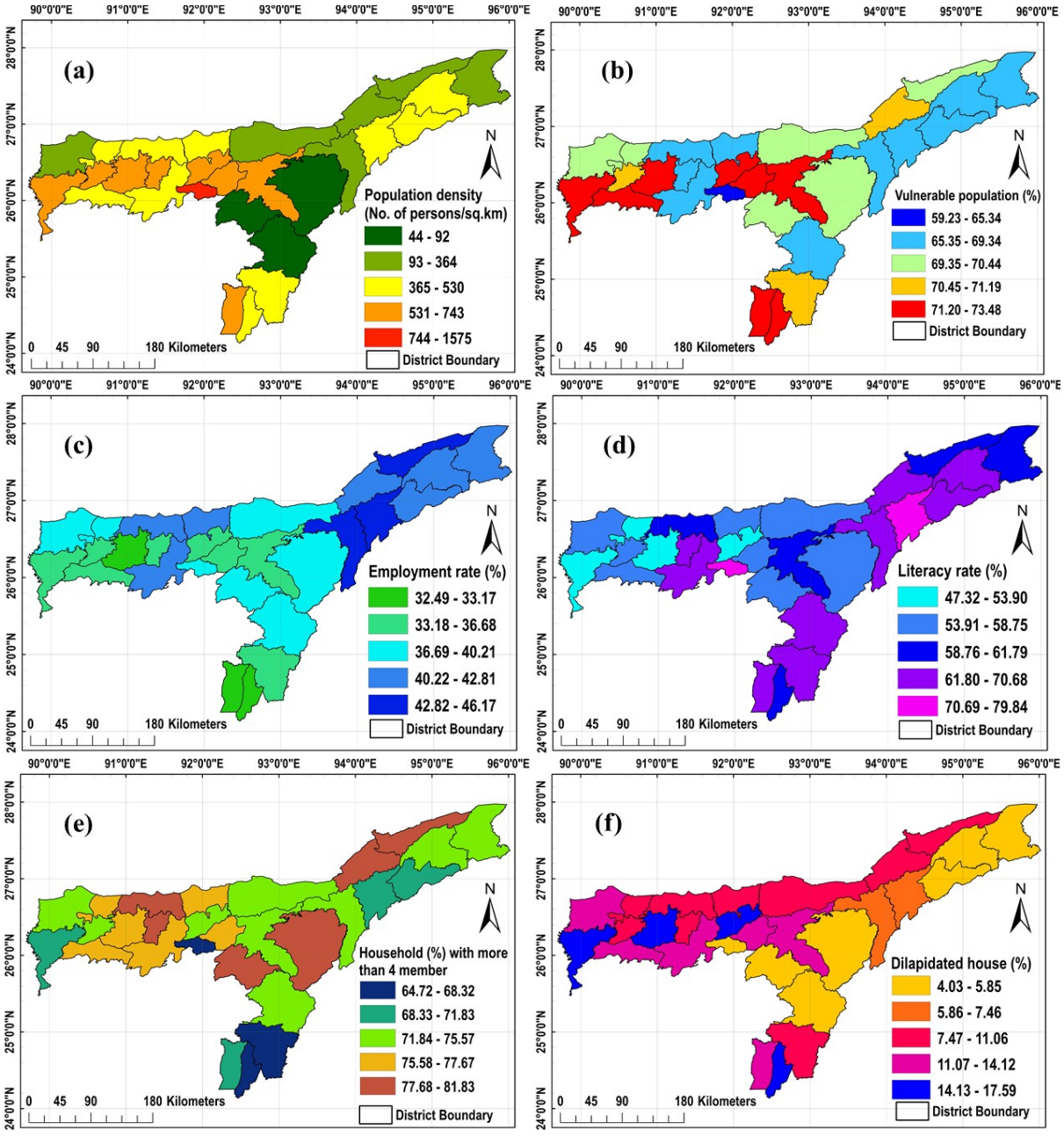

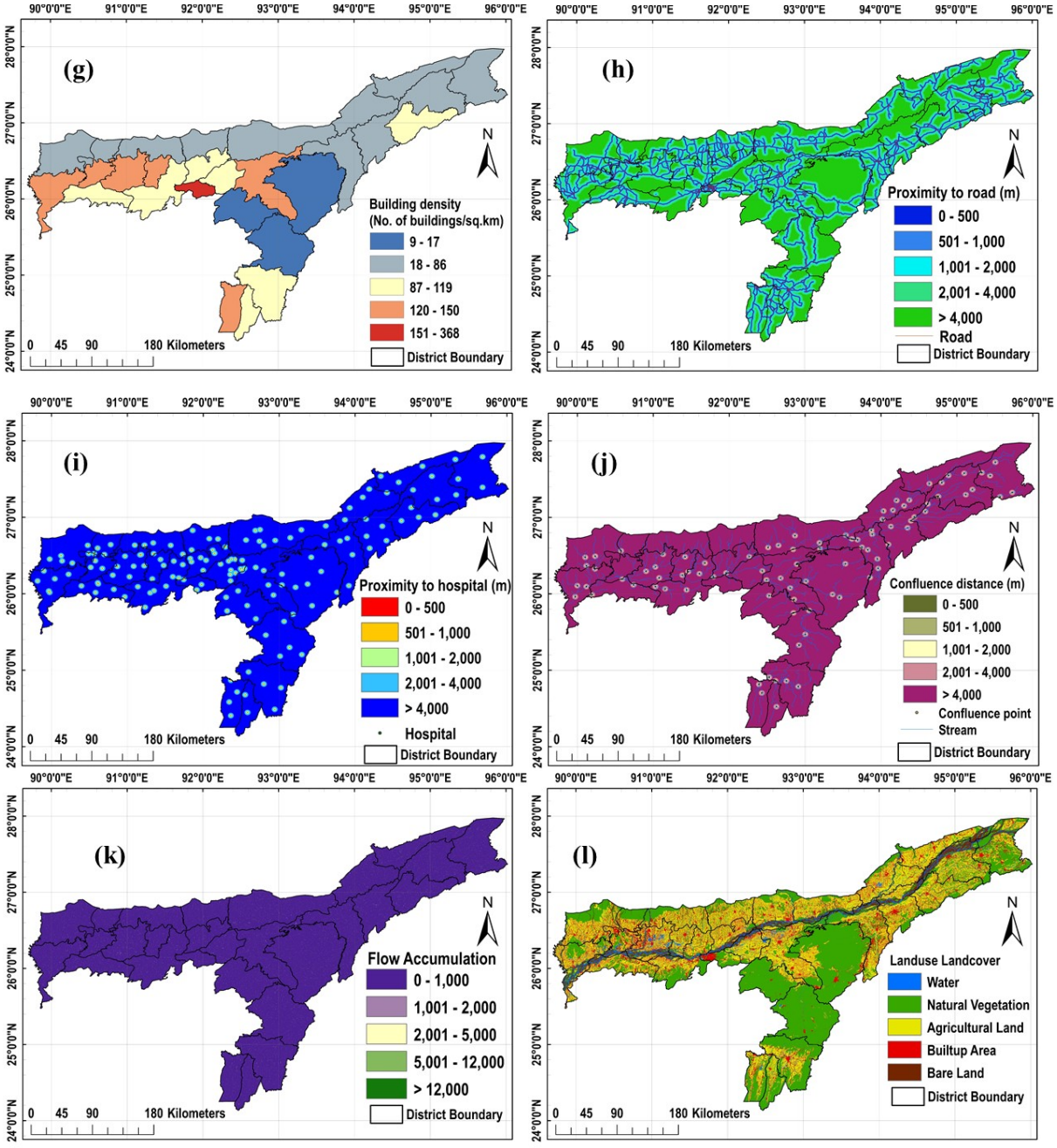

Figure 3. Flood vulnerability indicators (a) to (l) indicate population density; vulnerable population; employment rate; literacy rate; a household with more than 4 members; dilapidated house; building density; proximity to the road; proximity to the hospital; confluence distance; flow accumulation; and LULC.

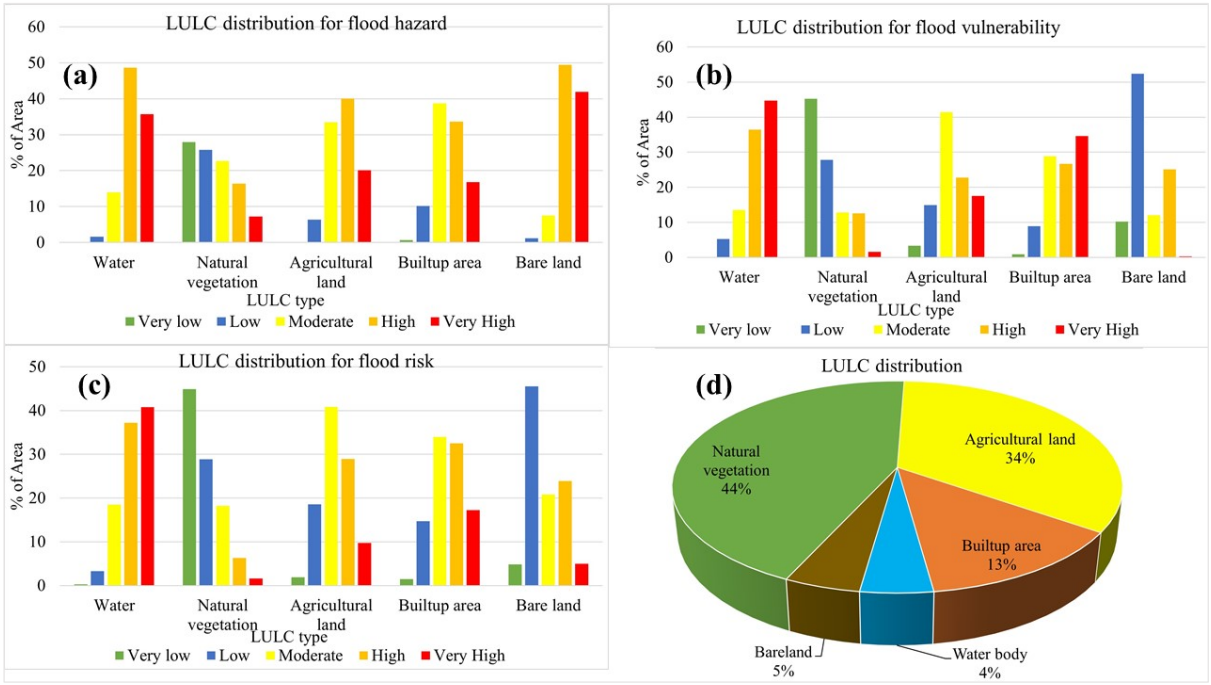

Figure 4. LULC area distribution for (a) Flood hazard; (b) Flood vulnerability; (c) Flood risk; and (d) LULC distribution.

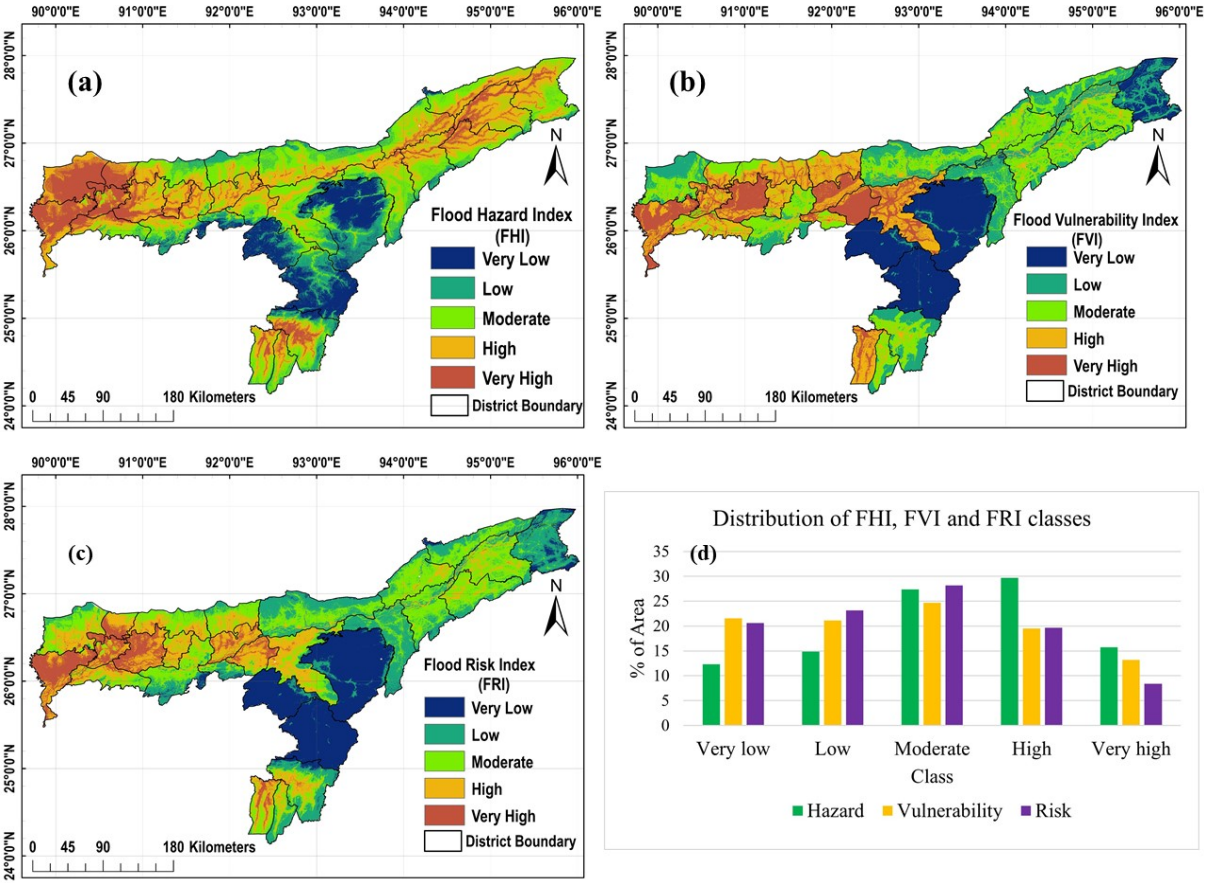

Figure 5. (a) Flood hazard index; (b) Flood vulnerability index; (c) Flood risk index; and (d) Area-wise distribution of FHI, FVI, and FRI.

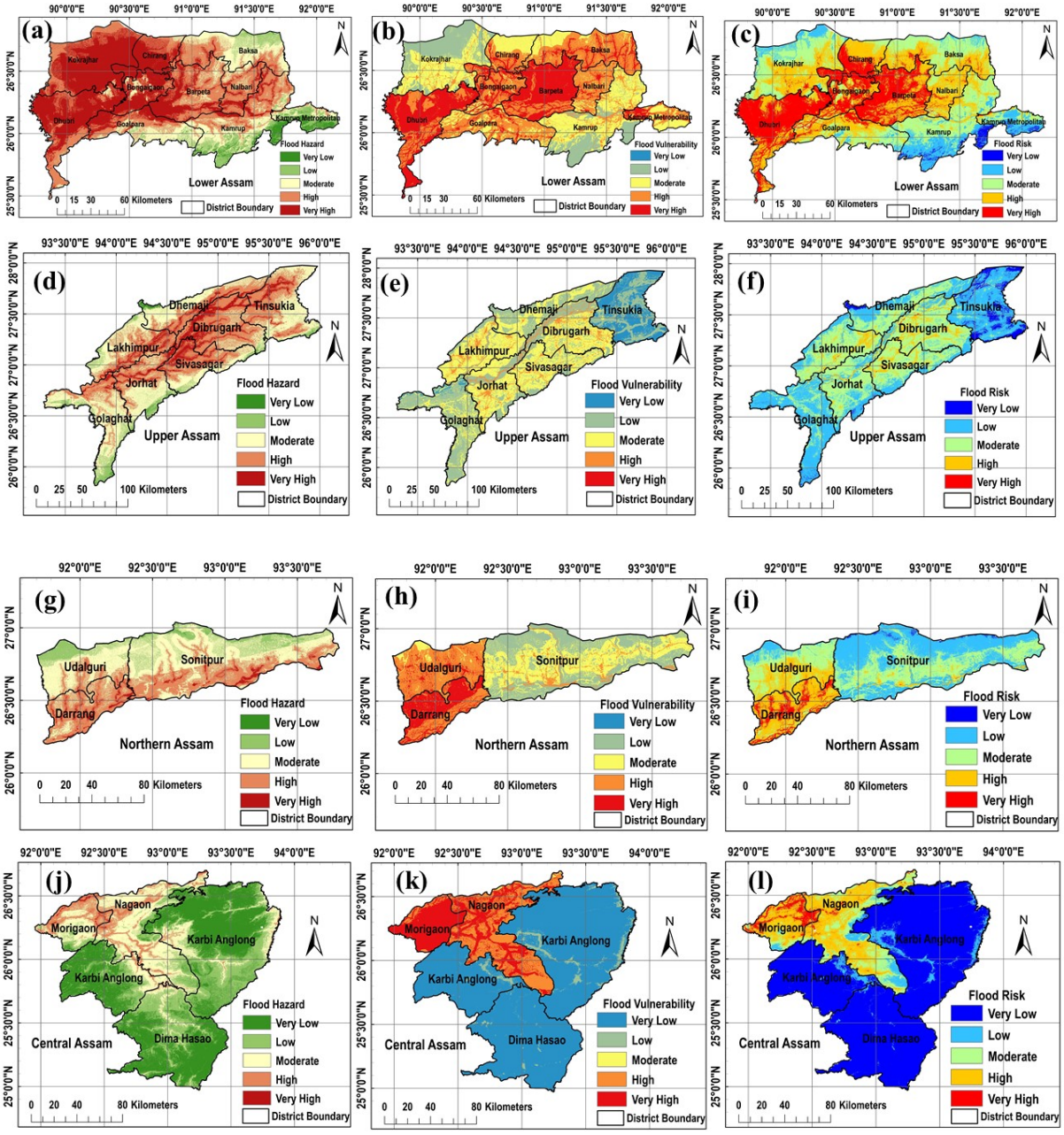

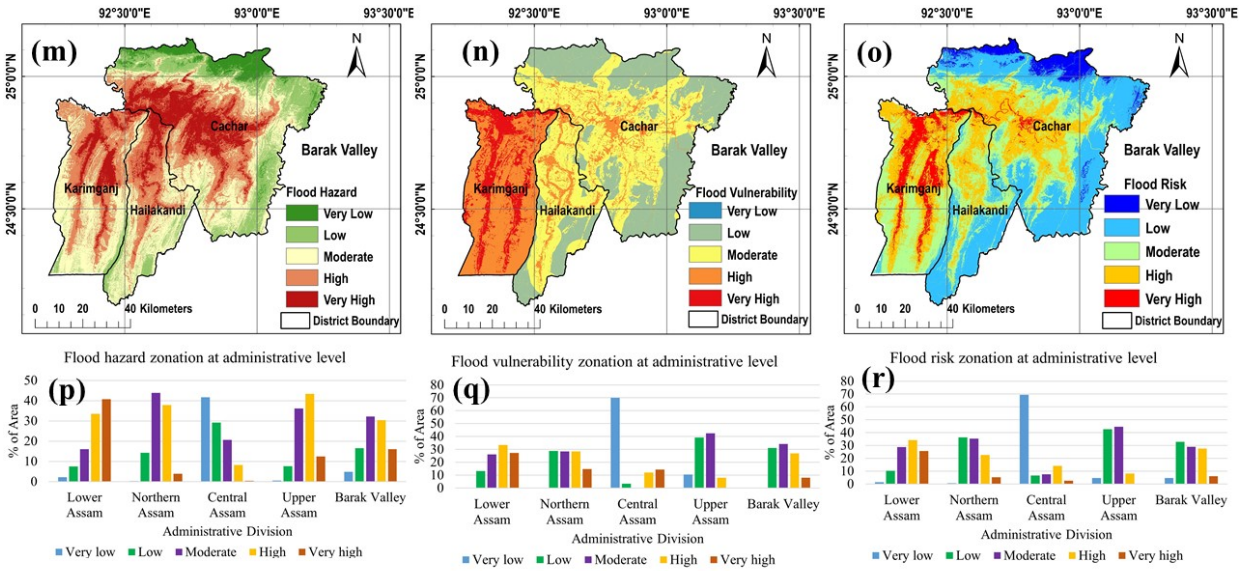

822

823 Figure 6. Flood profile of Assam at the administrative level (a) to (c) Lower Assam; (d) to (f)

824 Upper Assam; (g) to (i) Northern Assam; (j) to (l) Central Assam; (m) to (o) Barak Valley; and

825 (p) to (r) Area distribution of flood hazard, vulnerability, and risk.